ELSEVIER

Journal of Hazardous Materials 60 (1998) 89–104

JOURNAL OF HAZARDOUS MATERIALS

# Air emissions from exposed, contaminated sediment and dredged materials 2. Diffusion from laboratory-spiked and aged field sediments

R. Ravikrishna [a], K.T. Valsaraj [a,*], S. Yost [b], C.B. Price [b], J.M. Brannon [b]

[a] *Department of Chemical Engineering, Louisiana State University, Baton Rouge, LA 70803-7303, USA*
[b] *Environmental Laboratory, US Army Engineer Waterways Experiment Station, Vicksburg, MS 39181, USA*

Received 1 September 1997; received in revised form 31 October 1997; accepted 3 November 1997

**Abstract**

The mass transfer of three polycyclic aromatic hydrocarbons (naphthalene, phenanthrene and pyrene) and a heterocyclic aromatic hydrocarbon (dibenzofuran) from sediment to air was studied in a large-area flux chamber. A laboratory-spiked local (University Lake, UL) sediment and an aged contaminated field (Indiana Harbor Canal, IHC) sediment was used. The effects of initial sediment moisture content, and changing air relative humidity were investigated. For high moisture conditions in the UL sediment, the flux remained large whereas for low moisture conditions, there was a sharp decrease in flux as a result of surface drying of the sediment. Under similar air velocities and moisture conditions, the flux from the aged IHC sediment was considerably smaller than from the laboratory-spiked UL sediment. Whereas, the flux from laboratory-spiked UL sediment was predicted satisfactorily by a conceptual mathematical model, that from the aged IHC sediment did not agree with the model predictions. It was concluded that only a portion of the contaminant was available for desorption from the aged sediment due to the differences in the sorption characteristics of relatively fresh and aged contaminated sediments.


*Keywords:* Sediment; Air emissions; Soil gas transport

* Corresponding author. Tel.: +1 504 388 1426; fax: +1 504 388 1476; e-mail: kvalsar@lsuvm.sncc.lsu.edu

0304-3894/98/$19.00 
*PII* S0304-3894(97)00157-X

## 1. Introduction

Presently, approximately 14 to 28 million cubic yards of contaminated sediments are managed annually [1]. The remediation of contaminated sediments poses a significant problem. In many cases the strategy is sediment dredging and storage in a confined disposal facility (CDF). A CDF is a diked near-shore, island or land-based location. In a CDF, water drainage and evaporation lead to contaminated sediments that are exposed and can be sources of volatile and semi-volatile organic compounds to the atmosphere. The possibility of long term release of air pollutants has been recognized as a potential problem in CDFs. It is, therefore, important to estimate the release rates of contaminants in order to evaluate risk from exposure to the biota and humans. Temperature, air relative humidity and sediment moisture content play significant roles in the air emission rate [2]. Although models have been proposed, there is insufficient data at the present time to test the assumptions in the models [3–5].

Compounds that are sorbed to the sediment solids (mineral and organic matter) desorb and migrate through the pore spaces to the air boundary layer above the sediment. The sorption capacity of sediments is highly influenced by the moisture content. Sediments can be classified as 'dry' ($< 1\%$ w/w water content), 'damp' (2 to 4% w/w water) and 'wet' ($> 4\%$ w/w water) based on their relative sorption capacities for non-polar hydrophobic organic compounds [6]. Dry sediment has a large surface area for sorption dominated by mineral matter, and hence the pore air concentration of the organic contaminants will be low. However, increasing moisture leads to competition between water and organic molecules for sorption sites. Mineral matter preferentially sorbs water and displaces non-polar organic compounds. As a result, the pore air concentration of contaminants will increase. Soil scientists have recognized this phenomenon and have demonstrated this in field and laboratory experiments of pesticide volatilization from soils [7]. This phenomenon has been reviewed in the literature [3,8,9].

In a previous work, Valsaraj et al. [2] investigated the effects of drying sediment on the flux to air of several polycyclic aromatic hydrocarbon compounds. A thin sediment layer (4-mm depth) was used in a microcosm to clearly delineate the 'wet' and 'dry' states of the sediment as air was passed over it. The air relative humidity was alternated between 0 and 100% to simulate cyclic dry and wet conditions. It was observed that when dry air was passed over wet sediment, the flux was high initially and quickly became negligible when the entire sediment was dry. Upon increasing the air relative humidity, the flux increased. A mathematical model was constructed that considered these effects and was observed to predict the data satisfactorily. The primary variable in the model that influenced the emission rate was the retardation factor, Rf that changed by orders of magnitude between the 'wet' and 'dry' sediment conditions. The change in Rf was attributed to the change in the sediment-to-air partition constant for the organic compounds under 'wet' and 'dry' conditions.

In an actual CDF, the sediment depth will be large, and the water flux from the sediment can be maintained at a high level due to capillary rise. Therefore, it is necessary to evaluate the effects of sediment depth and varying initial sediment moisture conditions upon the air emission rate. The age of contamination in the sediment will also play a crucial role in determining the emission rate. In particular, it has been observed

that aging lead to encapsulation of contaminant within the sediment matrix. Thus, sorption and desorption follow different paths leading to hysteresis [10]. Laboratory-spiked sediments fail to show such behavior. Hence, it is important to contrast the air emission rates from aged and spiked sediments. With the above aims in mind, experiments were conducted in large flux chambers. Two sediments were used—a laboratory-spiked University Lake, Louisiana sediment and a naturally contaminated aged sediment from the Indiana Harbor Canal. Both sediments contained similar concentrations of polycyclic aromatic hydrocarbons.

## 2. Experimental

### *2.1. Flux chamber*

The design of the large flux chamber was broadly based on the design of the small microcosms used for the previous experiments [2]. The flux chamber was divided into a top and a bottom section. The total area of the sediment containing bottom section was 375 $cm^2$ and the total sediment depth was 10 cm. The top section was used to provide channels for airflow across the sediment surface. The entire unit was constructed out of anodized aluminum. Fig. 1 is a schematic of the flux chamber. The main objective of the design of the top section was to ensure uniform airflow at high air velocities. The main airflow was split into several channels using baffles. In order to achieve a uniform

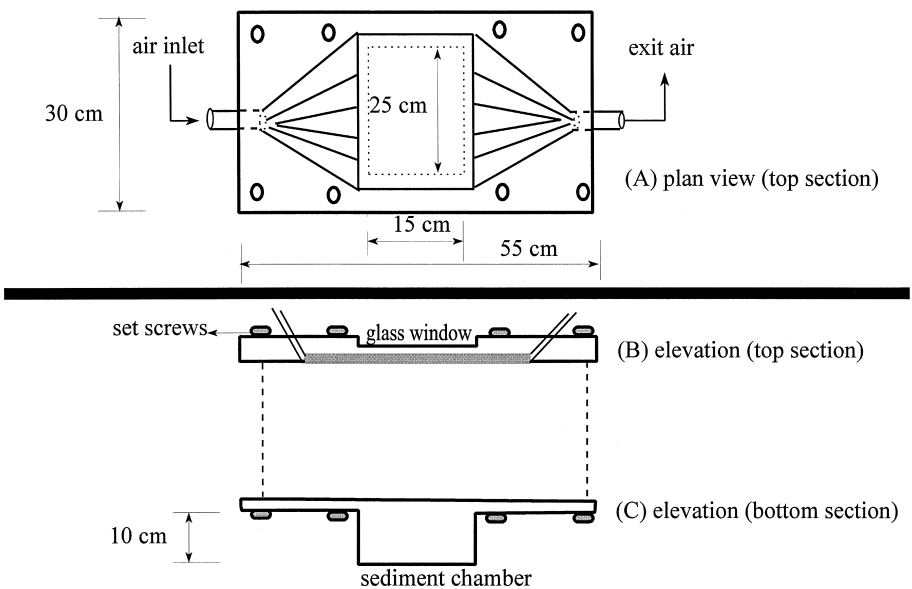


Fig. 1. Schematic of the large area flux chamber: (A) plan view (top section), (B) elevation (top section) and (C) elevation (bottom section).

airflow, a thin layer of gum was used to partially block some of the entrance channels. The flow profile was checked using a thin monolayer of Drierite© that substituted for the sediment surface, and passing humid air at the desired flowrate. The pattern of color change in the adsorbent was observed to ensure that a uniform air front was moving over the sediment surface. An air flow rate of 1.7 l/min was used in most of the experiments. This translated to a linear velocity of 5.67 cm/s. One experiment was conducted at a small linear airflow velocity of 0.33 cm/s.

### *2.2. Sediments and contaminants*

Two different sediments were used in these experiments. The first one was obtained locally from the University Lake (UL) in Baton Rouge, LA. This sediment was spiked in the laboratory with tracers, viz. polycyclic aromatic hydrocarbons (pyrene, phenanthrene and dibenzofuran) using a procedure described in an earlier work [11]. $NaN_3$ (Sodium azide) was added to the sediment to prevent biodegradation of PAHs. The second sediment used was aged, contaminated obtained from the Indiana Harbor Canal (IHC); this sediment contained several organic contaminants such as polycyclic aromatic hydrocarbons (PAHs), polychlorinated biphenyls (PCBs) and inorganic contaminants such as ammonia and hydrogen sulfide. The Indiana Harbor Canal sediment contained 0.9% oil and grease. We focused in this work only on the PAHs because of their widely prevalent nature in several CDFs. The properties of the two sediments are outlined in Table 1; the contaminant loading and properties are given in Table 2.

Table 1
Properties of sediments

| Property | UL sediment | | IHC sediment |
|---|---|---|---|
| | High moisture | Low moisture | |
| Clay (%) | 56 | 56 | 8 |
| Sand (%) | 3 | 3 | 45 |
| Silt (%) | 41 | 41 | 46 |
| Fraction organic carbon (%) | 4 | 4 | 2.6 |
| Fraction oil and grease (%) | NA | NA | 0.9 |
| Porosity, (−) | 0.7 | 0.44 | 0.79 |
| Bulk density ($g/cm^3$) | 0.67 | 1.7 | 0.6 |
| Initial moisture content (% w/w) | 48 | 25 | 54 |
| *Contaminant loading* | | | |
| DBF (mg/kg) | $66 \pm 4$ | $108 \pm 22$ | NA |
| NAPH (mg/kg) | NA | NA | 38 |
| PHE (mg/kg) | $65 \pm 5$ | $97 \pm 4$ | 51 |
| PYR (mg/kg) | $69 \pm 4$ | $94 \pm 5$ | 59 |
| TRPH (mg/kg) | NA | NA | 12,790 |

NA, not available or applicable.
Porosity and bulk density of the UL sediment (low moisture) measured after drying the sediment to the desired moisture content.
TRPH, Total Recoverable Petroleum Hydrocarbons.

Table 2
Contaminant properties

| Property | NAPH | DBF | PHE | PYR |
|---|---|---|---|---|
| Molecular weight | 128.18 | 168.20 | 178.24 | 202.26 |
| Aqueous solubility (mg/l) | 32 | 10 | 1 | 0.15 |
| Vapor pressure (mm Hg) | 0.017 | 0.0036 | 0.00025 | $4.5 \cdot 10^{-6}$ |
| Log $K_{oc}$ (1/kg) | 3.1 | 4.0 | 4.4 | 4.8 |
| Log $K_{ow}$ | 3.4 | 4.1 | 4.5 | 5.1 |
| Air diffusivity ($cm^2/s$) | 0.062 | 0.060 | 0.058 | 0.054 |
| Henry's constant, (−) | 0.019 | 0.0031 | 0.0025 | 0.00045 |

The literature values of Henry's constant, aqueous solubility and vapor pressure for these PAHs vary considerably between references. The above values are taken from Thoma [12].

### *2.3. Procedure*

A known amount of homogenized sediment was placed in the bottom section of the chamber ($\approx$ 9 to 9.5 cm deep). The surface of the sediment was smoothened with the help of a metal planing device that was also used for the purpose of sectioning the sediment. The top section was bolted into place. The contact between the sections was made airtight with vacuum grease and a Teflon gasket around the working area of the chamber. Compressed air from a cylinder was set to the desired flow rate and passed over the sediment surface. The relative humidity and temperature of the incoming air and outlet air were measured using a thermohygrometer (Cole–Parmer, IN) connected in-line with the help of a glass joint, which housed the instrument probe. Humid air was obtained by bubbling the air through a diffuser immersed in a water column.

### *2.4. Sampling and analysis*

A contaminant trap was attached in-line at the outlet at regular intervals for a fixed sampling time. The trap used for PAHs was made of XAD-2 resin (Orbo 43 from Supelco, PA) packed in a glass column. The trap was removed from the line at the end of a sampling interval. The adsorbent was then solvent extracted and analyzed using Standard Method 8310 [13].

Flux was calculated using the equation

$$N_A(t)\frac{\Delta m}{A_c \times \Delta t} \tag{1}$$

Where $\Delta m$ is the mass (ng) of compound collected on the trap in time $\Delta t$ (h). $A_c$ is the area of the sediment–air interface ($cm^2$).

## 3. Results and discussion

### *3.1. Mathematical models*

Mathematical models exist in the literature that can be used to estimate the volatilization of contaminants from exposed sediments (for example, see Ref. [14]).

The diffusion equation for a contaminant within the pore air space in the sediment is given by Ref. [15]

$$\frac{\partial C_A}{\partial t} = \frac{D_e}{R_f} \cdot \frac{\partial^2 C_A}{\partial z^2}. \tag{2}$$

The required boundary conditions are

$$\begin{aligned} &C_A(z,t)\big|_{t=0} = C_o^* && z \in [0,\infty] \\ &C_A(z,t)\big|_{z\to\infty} = C_o^* && t > 0 \\ &-D_e \frac{\partial C_A}{\partial z}\bigg|_{z=0} + k_a \cdot C_A(z,t)|_{z=0} = 0 && t > 0 \end{aligned} \tag{3}$$

$D_e$ is the effective diffusivity in the sediment pore space given by the Millington–Quirk [15] relationship ($D_A \varepsilon_a^{10/3}/\varepsilon_T^2$, $cm^2/h$). $C_o^*$ is the initial pore space concentration of the contaminant ($ng/cm^3$) and is given by $w_A/K_d^*$. $w_A$ is the sediment concentration of the contaminant ($ng/g$). $k_a$ is the mass transfer coefficient to air ($cm/h$) obtained from an established correlation for flow over a flat plate of length $d$ in the direction of airflow [15]. The correlation is $Sh = k_a d/D_A = 0.664\ Re^{0.5} Sc^{0.33}$, where $Re = d\ v/\nu$ and $Sc = \nu/D_A$ [16]. $\nu$ is the kinematic viscosity of air. $R_f$ is the retardation factor for the contaminant (dimensionless). The retardation factor is given by the following equation: $R_f = \varepsilon_a + \frac{\varepsilon_w}{H_c} + \rho_b K_d^*$, where $\varepsilon a = (1-\theta)\varepsilon_T$ is the air-filled porosity, and $\varepsilon_w = \theta \cdot \varepsilon_T$ is the water-filled porosity. $\theta$ is the water content. $\varepsilon_T$ is the total porosity of the sediment. Two boundary conditions and an initial condition are given above. A semi-infinite domain for the sediment is considered in one of the boundary conditions at the bottom of the chamber. A convective surface with an air phase mass transfer coefficient, $k_a$ is considered as the second boundary condition. Both $k_a$ and $R_f$ are assumed constant during the experiment.

The solution to the above diffusion equation is [17]

$$C_A(z,t) = C_o^* \cdot \left[ erf\left( \frac{R_f z}{\sqrt{4 D_e R_f t}} \right) + \exp\left( \frac{k_a z}{D_e} + \frac{k_a^2 t}{D_e R_f} \right) \cdot \operatorname{erfc}\left( \frac{R_f z}{\sqrt{4 D_e R_f}} + k_a \cdot \sqrt{\frac{t}{D_e R_f}} \right) \right]. \tag{4}$$

The flux from the sediment to air is

$$N_A(t) = C_o^* \cdot \left[ k_a \cdot \exp\left( \frac{k_a^2 t}{D_e R_f} \right) \cdot \operatorname{erfc}\left( k_a \cdot \sqrt{\frac{t}{D_e R_f}} \right) \right]. \tag{5}$$

For a finite sediment of depth $H$, the semi-infinite boundary condition has to be changed. The flux of the contaminant from the sediment-to-air in this case is given by the following equation [2]

$$N_A(t) = \frac{2 D_e C_o^* L^2}{H} \cdot \sum_{n=1}^{\infty} \frac{\exp\left[ \dfrac{-\alpha_n^2 D_e t}{H^2 R_f} \right]}{L(L+1) + \alpha_n^2}. \tag{6}$$

In the above equation, $L = k_a H/D_e$. $\alpha_n$ is the nth eigen value of the equation $\alpha \cdot \tan \alpha = L$. Eqs. (5) and (6) give identical results if the bottom boundary condition does not influence the flux from the surface. This occurs in those cases where the depth of the sediment layer is large and the surface depletion is small. These equations suggest that there are two resistances to mass transfer. Initially ($t = 0$) the resistance is completely on the air-side and flux is $k_a C_o^*$. With time, it becomes more sediment-side diffusion controlled. For a predominantly diffusion controlled situation, the flux varies as $1/\sqrt{t}$ if both $D_e$ and $R_f$ remain unchanged.

### 3.2. Experimental results

#### 3.2.1. Water flux from low and high moisture UL sediment

Fig. 2A shows the flux of water from the UL sediment to air at the airflow velocity of 5.67 cm/s. The initial sediment moisture content was 48% (w/w). The initial water flux from the sediment was 0.006 g/cm$^2$ h, which declined to a steady value of 0.005 g/cm$^2$ h in 48 h. The inlet air had 0% RH while the exit air during this phase was at a relative humidity of 80–90%. Fig. 2B shows the moisture profile in the sediment at the end of 568 h of experiment. Both the horizontal profile (in the direction of air flow) and vertical profile are shown. It was estimated from the sediment moisture profile that approximately, 720 g of water was lost during the experiment. The sediment moisture remained high even after 568 h. The moisture content near the air inlet was small and progressively increased towards the exit section of the chamber. The average moisture content of the surface sediment was 8% (w/w), and for the bottom sediment was 13% (w/w). We, therefore, concluded that the surface sediment contained sufficient moisture throughout the experiment to maintain 'wet' conditions. It was also observed from the

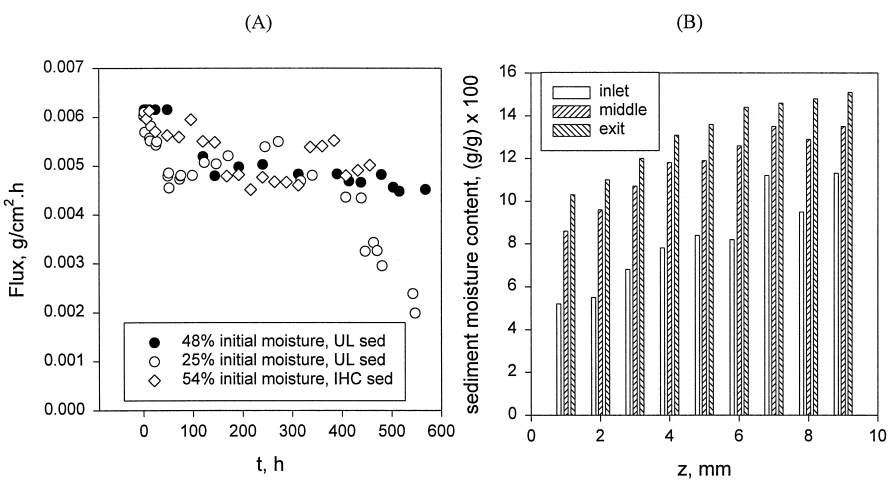


Fig. 2. (A) Water flux from the UL and IHC sediments. (B) Moisture content with depth for the experiment involving 48% moisture UL sediment at the end of the run.

sediment profile that a gradient existed only in the first 10 mm of the sediment layer, while the deeper sediment (> 10 mm) maintained a constant moisture content.

Fig. 2A also shows the flux of water from the UL sediment that contained a low initial moisture content (25% w/w). The air velocity was 5.67 cm/s in this case as well. The water flux was similar to that at the higher moisture content, but decreased after about 400 h indicating a significant decrease in surface moisture content. There is thus a period of constant drying rate followed by a falling rate. During the *constant drying rate* period, the capillary rise of water from deeper layers was able to replenish the water lost from the surface. During the *falling rate* period, the residual moisture was lost from the surface at a rate faster than the capillary rise. We also observed that during this experiment, a distinct 'drying front' formed near the air inlet and, the surface was completely dry when the water flux began to decrease.

### *3.2.2. Flux of contaminants from high moisture UL sediment*

Fig. 3 is a comparison of the fluxes of three compounds (DBF, PHE and PYR) from the high moisture UL sediment. Dry air at 0% RH was used in this case. The fluxes were in the order DBF > PHE > PYR. The sediment–air partition constants, the Henry's constant and vapor pressure all vary in the order DBF > PHE > PYR. The DBF flux decreases from an initial value of 32 ng/cm$^2$ h to a low value of 12 ng/cm$^2$ h in 48 h, while that of PHE decreased from 7 ng/cm$^2$ h to 3.5 ng/cm$^2$ h in the same period. PYR flux, however, remained constant at ~ 0.8 ng/cm$^2$ h during the run. This trend is in contrast to that observed during previously reported experiments with a thin sediment layer where the flux decreased drastically due to surface drying and resulting change in the retardation factor [2]. The near-constancy in PHE and PYR flux observed in the present experiment indicated that a significant portion of the resistance to mass transfer

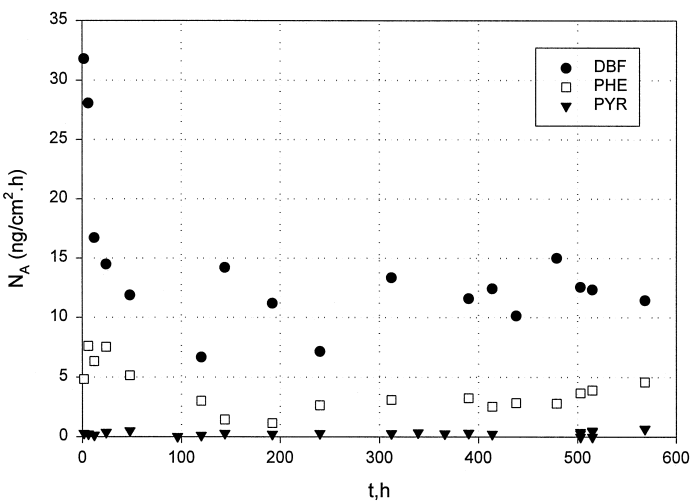


Fig. 3. Experimental data on the flux of DBF, PHE and PYR from the 48% moisture UL sediment. Dry air was passed over the wet sediment.

for these chemicals resided in the air phase (air boundary layer). Only for DBF was the flux predominantly sediment-side controlled after the initial period. In order to illustrate this point consider the time taken for the two resistances to become equal which is given by $\tau^* = \frac{D_e R_f}{3k_a^2}$ (see Ref. [15] for details). Since $R_f$ is much larger for PYR than for DBF, sediment-side control will take longer to achieve for PYR than for DBF. Increasing $k_a$ (which is proportional to the square root of the air velocity) will accelerate the achievement of sediment-side control for diffusional mass transfer.

Fig. 4A shows the flux of dibenzofuran (DBF) from the University Lake sediment (48% initial moisture content) at two superficial airflow velocities of 5.67 (flow rate of 1700 ml/min) and 0.33 cm/s (flow rate of 100 ml/min). Inlet air was dry (0% RH). At the low airflow velocity, the DBF flux was distinctly small throughout the length of the experiment. The DBF flux at the high air velocity was large ($\sim$ 32 ng/cm$^2$ h) initially and decreased to an almost constant value of $\sim$ 12 ng/cm$^2$ h after 48 h. DBF flux to air is composed of two components—an advective flux due to water evaporation and diffusion through the pore air space. The contribution to DBF flux due to water evaporation from the surface is small. For example, if we consider a constant water evaporation flux of 0.005 g/cm$^2$ h and pore water DBF concentration of $1.2 \cdot 10^{-4}$ mg/cm$^3$, the flux of DBF would be only 0.67 ng/cm$^2$ h, which is negligible in comparison to the observed flux. We, therefore concluded that the DBF flux was predominantly due to pore air diffusion within the sediment. The increase in flux with increasing air velocity indicated that a significant resistance to mass transfer existed in the air boundary layer above the sediment at the low air velocity. Increasing air velocity decreases the thickness of the air boundary layer and increases the flux.

Fig. 4A also shows the predicted flux from Eq. (5) for DBF from the UL sediment at the high air velocity. The model over-predicted the flux. The one variable in the model

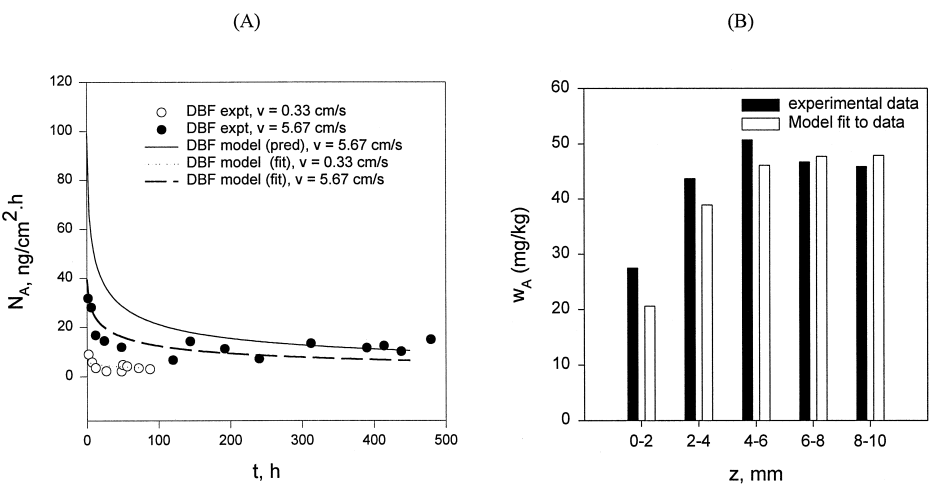


Fig. 4. (A) Experimental and model (predicted and fitted) DBF flux vs. time data for 48% moisture UL sediment. Dry air was passed over wet sediment. (B) Experimental and model fit data on the DBF concentration on sediment with depth at the end of the run.

Table 3
Sediment–air partition constant for DBF on UL sediment

| Sediment condition | Predicted | Model-fitted |
|---|---|---|
| 'Wet' sediment (log $K^*_{dw}$) | 5.11 | 5.50 |
| 'Dry' sediment (log $K^*_{dd}$) | 7.04 | 6.46 |

Predicted values of $K^*_{dw}$ and $K^*_{dd}$ obtained as described by Valsaraj et al. [2].
Note that the model-fitted values are only applicable for the selected values of $k_a$ and $D_e$ used for the simulations.

that has the largest uncertainty is the retardation factor, $R_f$ as a result of the uncertainty in $K^*_d$. The error in estimated $K^*_d$ $(=K_{oc} f_{oc}/H_c)$ arises from the uncertainty in reported $H_c$. For example, for DBF, no reported experimental values of $H_c$ exist. The chosen value is the ratio of vapor pressure to aqueous solubility, both of which span a wide range. For PHE, the reported values vary between $8 \cdot 10^{-4}$ and $2 \cdot 10^{-3}$ at 298 K [18]. Hence, we are justified in adjusting $R_f$ (i.e $K^*_d$) to obtain a better fit of the model to the experimental data. The model fitted curve is also shown in Fig. 4A. The predicted and fitted $K^*_d$ values are shown in Table 3. For DBF, the fitted value is $2.5 \cdot$ larger than predicted. Since the sediment conditions remained 'wet' for the duration of this experiment, the sediment–air partition constant obtained from the model-fit are for the 'wet' sediment which we shall designate, $K^*_{dw}$.

Fig. 4B shows the sediment concentration profile for DBF after 568 h of the experiment. Both experimental and model-fitted profiles are shown. Eq. (4) was used to obtain the model fitted profile with depth. The flux in Fig. 4A and the sediment profile in Fig. 4B are independent measurements, but were fitted using the same values of $R_f$.

After 568 h of the experiment involving dry air at a superficial velocity of 5.67 cm/s over the UL sediment, the relative humidity of incoming air was increased to 90%. If the surface sediment had been dry, then one would anticipate an increase in flux due to the change in $R_f$ from 'wet' to 'dry' sediment conditions, as was shown in a previous work with a thin sediment layer [2]. In the present case (not shown here), there was no discernible change in flux as a result of the change in air relative humidity. This showed that as long as the water flux at the sediment surface was maintained, the air relative humidity had no effect on the overall flux from the sediment to air.

### *3.2.3. Flux of contaminants from low moisture UL sediment*

Fig. 5 shows the flux of DBF, PHE and PYR from the low moisture (25% w/w) laboratory-spiked UL sediment. The effect of change in relative humidity after 510 h is also noted. The initial flux of DBF in this case was 111 ng/cm$^2$ h while that of PHE and PYR were 13 and 0.8 ng/cm$^2$ h, respectively. Since flux is proportional to the initial sediment concentration (Eq. (5)) and since the initial concentrations were larger in this case than for the high moisture sediment, the large flux values were reasonable. More importantly, the sharp change in flux unlike the high moisture case was a significant observation. The DBF flux showed a sharp decline from a high value of 111 to 10 ng/cm$^2$ h in 50 h; thereafter it remained somewhat constant. The PHE flux

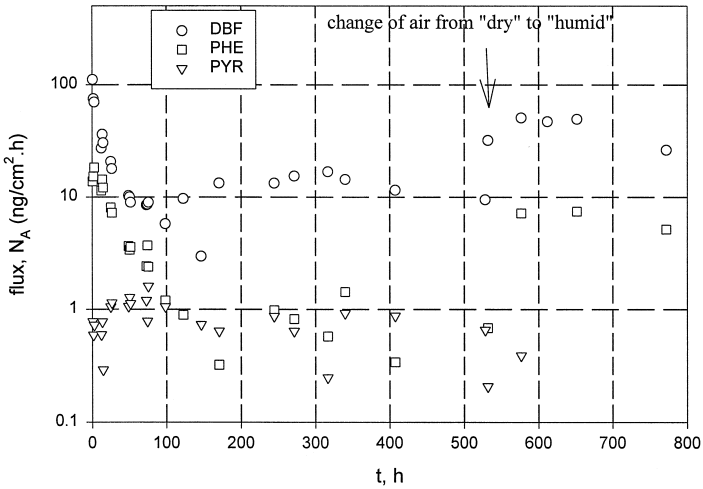


Fig. 5. Experimental data on the flux of DBF, PHE and PYR from the 25% moisture UL sediment. Dry air was passed over the wet sediment. At 532 h the air relative humidity was changed to 97%.

showed a similar profile (13 to 3 ng/cm$^2$ h). PYR, however showed a constant flux of $\approx$ 1 ng/cm$^2$ h throughout the experiment. It was clear from the flux data that PYR was air-phase controlled, while DBF was predominantly sediment-side controlled. It was also clear that for DBF the flux was *not* proportional to $1/\sqrt{t}$. We attribute this behavior solely to the changing $R_f$ as a result of the drying of the sediment. Note that in Fig. 2A, the water flux from the 25% moisture sediment showed a distinct decrease after 400 h. Although during the first 400 h, water flux was constant, there was a visible 'drying front' that formed at the air inlet and progressed towards the outlet. The flux from the dry regions of the sediment will be very low and hence the overall flux from the sediment will decline rapidly as the surface sediment underwent drying. This observation was clearly evident for the thin sediment case that we reported earlier [2]. In the high sediment moisture case, we did not observe such a 'drying front' even at the end of the experiment. Further proof for drying sediment is the influence of RH upon the flux of PAHs as shown in Fig. 5. Unlike the previous case of high sediment moisture, in this case a distinct increase in flux was noted upon changing to humid air. This was also clearly demonstrated in our earlier work [2]. The flux of DBF increased to 50 while that of PHE increased to 10 ng/cm$^2$ h and then declined slowly thereafter.

Fig. 6 shows, for example, the experimental and model predicted values of flux for DBF. The initial flux predicted using the $K^*_{dw}$ obtained from the fit to the earlier data (Table 3) was in good agreement with the experimental data. This is to be expected since initially the sediment is 'wet' and the model for the wet sediment should apply. The long-term flux in this case cannot be predicted using the same model, since the sediment had undergone complete drying. In fact, the long term flux from the 'wet' sediment model was considerably higher than experimental as shown in Fig. 6. For the long-term flux the 'dry' sediment conditions should apply, i.e. it is a function of the

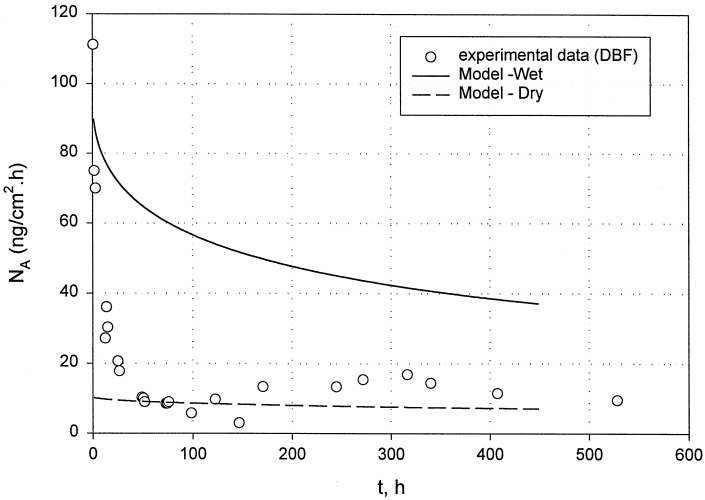


Fig. 6. 'Wet' and 'Dry' model data for DBF flux compared to experimental data on 25% moisture UL sediment. Dry air was passed over the wet sediment.

sediment–air partition constant under 'dry' conditions which we will designate, $K^*_{dd}$. By fitting the flux at long times to Eq. (5) modified for 'dry' conditions, we obtained a model fit value of $K^*_{dd}$. In order to do so, we used $R_f = \varepsilon_a + \rho_b K^*_{dd}$ and $D_e = D_A \varepsilon_a^{4/3}$ as in the earlier work [2]. The model fitted value of $K^*_{dd}$ can be compared to the predicted value of $K^*_{dd}$ and is shown in Table 3. The model fit value was only 25% of the predicted value. The predicted value was based on a theoretical estimate of the monolayer adsorption capacity, $W_A^*$ of the sediment for the contaminant [2]. Significant uncertainty in the monolayer capacity term can result in large changes in predicted $K^*_{dd}$ such as reflected in the model fit $K^*_{dd}$ value.

### *3.2.4. Flux of contaminants from high moisture IHC sediment*

For the IHC sediment, after the passage of dry air over the initially wet sediment (54% w/w moisture) for 14 days, the air relative humidity was switched to 97% and continued for 7 days. Fig. 7 shows the flux of NAPH, PHE and PYR during the run The superficial air velocity was 5.67 cm/s. The initial flux of naphthalene was larger than that of phenanthrene and pyrene. The flux of NAPH decreased from $46 \pm 8$ ng/cm$^2$ h to a low value of 0.05 ng/cm$^2$ h in 168 h. Similarly, the flux of PHE decreased from its initial value of $1.9 \pm 1.4$ ng/cm$^2$ h in 168 h. The decrease in flux reached a quasi steady-state value for both compounds. The change in air relative humidity that occurred after 14 days did not have any effect on the flux of any of the PAHs. Sediment moisture flux was monitored during this experiment and was observed to remain large ($\approx 0.0048$ g/cm$^2$ h) throughout the run. Since the surface sediment was moist, we concluded that the compounds did not experience a change in $R_f$ sufficient enough to cause a change in flux. The flux of pyrene was constant throughout the experiment indicating that it was predominantly air-phase controlled.

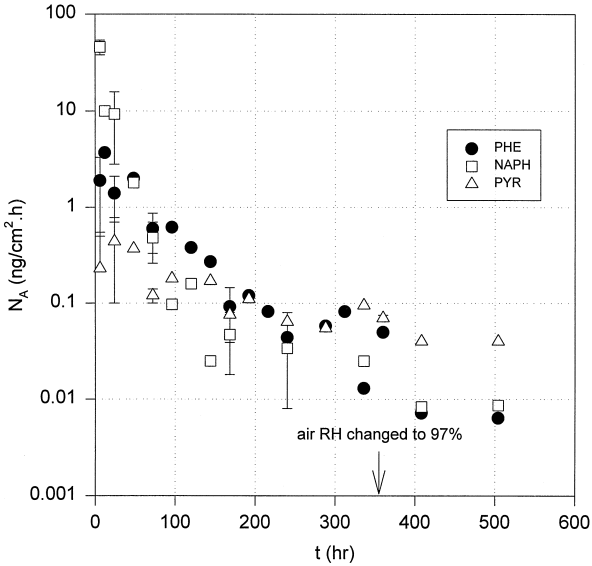


Fig. 7. Experimental data on the flux of NAPH, PHE and PYR from the 54% moisture IHC sediment. Dry air was passed over the wet sediment. Air relative humidity changed to 97% at 342 h.

Phenanthrene is a contaminant in both UL and IHC sediments. The initial sediment concentrations in both cases were similar and so was the initial moisture content. Whereas the UL sediment was silty–clayey, the IHC sediment was silty–sandy. The organic carbon fraction was 4% for UL and 2.6% for IHC sediment. However, IHC sediment contained about 0.9% oil and grease whereas UL sediment did not. UL was a laboratory-spiked sediment while IHC was an aged contaminated sediment. Since similar air velocities were used in both cases, the atmospheric boundary layer resistance was also comparable. The model (Eq. (5)) then predicted PHE fluxes that were smaller for IHC than UL sediment. (Fig. 8). The sediment–air partition constant $K^*_{dw}$ used for the simulations were $2.5 \cdot 106$ l/kg for the UL sediment and $2.2 \cdot 106$ l/kg for the IHC sediment. All other parameters used are given in Tables 1 and 2. The predicted values are in good agreement with the experimental values for the UL sediment. For the IHC sediment, model predictions are orders of magnitude larger than observed values.

A qualitative comparison of the experimental PHE fluxes (Fig. 8) led to two important observations. Firstly, the magnitude of the flux was small for the IHC sediment in comparison to that from UL sediment. There is a large amount of accumulating evidence in support of the fact that for aged sediments a large fraction of the contaminant is irreversibly bound to the sediment particles [10,19–21]. Aging is said to involve diffusion into soil micropores, partitioning into soil organic matter, strong surface adsorption or a combination of all these processes. The existing theory is that one can conceptualize the aged sediment to be composed of two compartments. The first compartment contains the labile fraction of the contaminant in equilibrium with the pore air space and characterized by the equilibrium sorption constant, $K^*_d$. The second

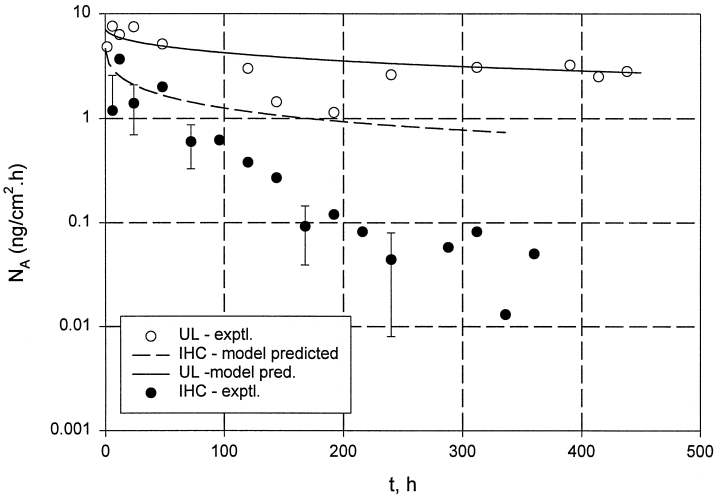


Fig. 8. Comparison of DBF flux from UL and IHC sediments. The UL sediment had an initial moisture content of 48%, while IHC had 54% moisture content. Dry air was passed over the wet sediment. Model predictions for the 'wet' sediments are also shown.

compartment contains resistant or tightly bound fraction for which adsorption kinetics is very slow. For a laboratory-spiked sediment, the aging process may not be long enough to produce a significant non-labile fraction, and hence desorption proceeds at the same rate as adsorption; the process is then characterized by a singular sorption constant, $K_d^*$.

The second important observation was that in the case of the IHC sediment, the flux sharply decreased reaching a quasi steady-state value at long times. There are several possible reasons for the sharp decrease in flux. One possible explanation is the formation of a dry layer of sediment near the surface as a result of water evaporation. The dry layer formed will have a large retardation factor and hence any material diffusing from the wet layer below will be trapped in the dry sediment. If a dry layer had formed, then a change in air relative humidity to 97% should have increased the flux [2]. Since this did not occur, we concluded that the dry layer formation was not the cause for the sharp decrease in flux from the IHC sediment. Additionally, the water evaporation rate from the surface was maintained at $\sim 0.0048\ g/cm^2\ h$ throughout the duration of the experiment.

Another explanation involves the effect of oil and grease in the IHC sediment upon the evaporation of PAHs. If the surface sediment was partly oil-film covered, evaporation from the surface oil layer would occur rapidly. The mass transfer from the oil layer will manifest as a first order (exponential) decay. Following evaporation from the oil film, a quasi steady-state diffusive flux from the sediment surface occurs. This contributes to a low mass transfer rate depending on the air–sediment partition constant and will be sediment-side diffusion controlled. Additionally, for the sediment particles that are oil-film coated, once the initial flux from the oil film rapidly decays, the subsequent stage will involve diffusion of contaminant from sediment to air through the oil film; a

process several orders of magnitude slower than diffusion through the pore air space. Experiments on other PAH-containing sediments with no oil and grease should be performed to test this hypothesis.

## 4. Conclusions

The behavior of aged IHC sediment vis-à-vis the laboratory inoculated UL sediment has important implications as far as estimation of air emission flux is concerned. It appears that air emission from the aged IHC sediment is distinctly lower than predicted by volatile flux models. This means that models for exposure developed through calibrations on laboratory inoculated sediments will overpredict contaminant exposure associated with dredged material. Therefore, appropriate models for aged sediment should be developed. These aspects are being currently pursued in our laboratory.

## Acknowledgements

The work at LSU was supported by grants from the U.S. EPA through the Hazardous Substance Research Center (South & Southwest) and the U.S. Army Corps of Engineers. At the U.S. Army Engineer Waterways Experiment Station, the work was supported by the Long-Term Effects of Dredging Operations (LEDO) program and the U.S. Army Engineer District, Chicago, IL.

## References

[1] Contaminated Sediments in Ports and Waterways—Cleanup Strategies and Technologies, National Research Council, NRC Press, WA, 1997.
[2] K.T. Valsaraj, B. Choy, R. Ravikrishna, L.J. Thibodeaux, D.D. Reible, C.B. Price, J.M. Brannon, T.E. Myers, J. Hazard. Mater. 54 (1997) 65.
[3] L.J. Thibodeaux, Theoretical methods for volatile emissions from dredged materials—comparison of predicted and laboratory measurements for New Bedford Harbor Sediment, Memorandum for Record, U.S. Army WES, Vicksburg, MS, Contract No. DACW39-89-M0207, 1989.
[4] K.T. Valsaraj, L.J. Thibodeaux, D.D. Reible, ASTM STP 1293 (1995) 227.
[5] U.S. Environmental Protection Agency, Assessment and remediation of contaminated (ARCS) sediments program—estimating contaminant losses from components of remediation alternatives for contaminated sediments, EPA 905-R96-001, Great Lakes National Program Office, Chicago, IL, 1996.
[6] K.T. Valsaraj, L.J. Thibodeaux, J. Hazard. Mater. 19 (1988) 79.
[7] W.F. Spencer, W.J. Farmer, W.A. Jury, Environ. Toxicol. Chem. 1 (1982) 17.
[8] C.T. Chiou, T.D. Shoup, Environ. Sci. Technol. 19 (1985) 1196.
[9] C.T. Erkey, J.F. Campagnolo, A. Akgerman, Sep. Purif. Meth. 24 (1995) 129.
[10] A.T. Kan, G. Fu, M.B. Tomson, Environ. Sci. Technol. 28 (1994) 859.
[11] D.D. Reible, V. Popov, K.T. Valsaraj, L.J. Thibodeaux, F. Lin, M. Dikshit, M.A. Todaro, J.W. Fleeger, Water Res. 30 (1996) 704.
[12] G.J. Thoma, Ph.D. Dissertation, Louisiana State University, Baton Rouge, LA, 1992.

[13] U.S. EPA, Test methods for evaluating solid waste—physical and chemical methods, SW-846, 2nd edn., NTIS, Springfield, VA, NTIS No. PB87-120291, 1982.
[14] R.G. Thomas, in: W.J. Lyman, R.E. Reehl, D.H. Rosenblatt (Eds.), Handbook of Chemical Property Estimation Methods, American Chemical Society, Washington, DC, 1990, pp. 16–1, 16–50.
[15] L.J. Thibodeaux, Environmental Chemodynamics, 2nd edn., Wiley, New York, NY, 1996.
[16] E.L. Cussler, Diffusion, 2nd edn., Cambridge Univ. Press, New York, NY, 1997.
[17] J.C. Crank, The Mathematics of Diffusion, 2nd edn., Oxford Univ. Press, New York, NY, 1975.
[18] D. Mackay, W.Y. Shiu, K.C. Ma, Illustrated Handbook of Physical–Chemical Properties and Environmental Fate for Organic Chemicals, Vol. 2, Polyaromatic Hydrocarbons, CRC Press, Boca Raton, FL, 1992.
[19] D.R. Shonnard, R.L. Bell, A.P. Jackman, Environ. Sci. Technol. 27 (1993) 457.
[20] M.D.F. Askari, M.P. Maskarinec, S.M. Smith, P.M. Bean, C.C. Travis, Anal. Chem. 68 (1996) 3431.
[21] P.B. Hatzinger, M. Alexander, Environ. Sci. Technol. 29 (1995) 537.